Supplementary Material for: "Strong van der Waals adhesion of a polymer film on rough substrates"

Juliane Klatt,*,† Pablo Barcellona,† Robert Bennett,† Olga S. Bokareva,‡ Hagen Feth,¶ Andreas Rasch,¶ Patrick Reith,¶ and Stefan Yoshi Buhmann†

†*Physikalisches Institut, Albert-Ludwigs-Universität Freiburg, Hermann-Herder-Str. 3, 79104 Freiburg, Germany*

‡*Institut für Physik, Universität Rostock, Albert-Einstein-Str. 23-24, 18059 Rostock, Germany*

¶*TrueDyne Sensors AG, Christoph-Merian-Ring 20, 4153 Reinach, Switzerland*

§*Freiburg Institute for Advanced Studies, Albert-Ludwigs-Universität Freiburg, Albertstr. 19, 79104 Freiburg, Germany*

E-mail: juliane.klatt@physik.uni-freiburg.de

A: Monomer Polarisabilities

We calculate the polarisabilities of ECTFE monomers (saturated with two additional hydrogen atoms for neutrality) by means of quantum chemical approach based on a response formalism as implemented in the Turbomole computational package [18]. Two different conformers of the ECTFE monomer exist. However, they show almost exactly identical responses when averaging over all possible orientations. For the calculation of the monomer polarisability, we have employed a hybrid density functional method combining Becke's exchange part

[19] and the Lee, Yang, and Parr correlation term [20] with Dunning's correlation-consistent basis set of triple-ζ quality [21] (B3LYP/cc-pVTZ) whereas all test computations have been done with a PBE/def2-SV(P) combination.

B: Determination of equilibrium distances

The equilibrium distance between the ECTFE polymer and the substrate are determined from a competition between local chemical binding and long-range dispersion forces. We evaluate the covalent interactions between ECTFE monomers and substrate surfaces by means of a hybrid density functional combined with a spin-valence double-ζ Pople basis set [22] B3LYP/6-31G(d) as implemented with the Gaussian 09 package [23]. To correctly predict the binding energy, the counterpoise correction method by Boys and Bernardi [24] has been applied to eliminate the basis set superposition error (BSSE) [25]. For the case of a (001) silicon surface with 2-1 reconstruction, two different silicon cluster sizes have been considered: $Si_{31}H_{28}$ and $Si_{45}H_{34}$. For both clusters, three starting positions of monomer relative to the surface have been chosen, leading to three different optimal structures for each case. The corresponding equilibrium distances range from 2.6–3.7Å justifying the use of an average distance.

To transfer our results to different substrates, a correction accounting for size-effects is introduced. It has been derived by comparing the nearest distances in optimized complexes with the sum of known atomic properties as covalent and van der Waals radii. For orientations 1 and 2, the F-Si bond is approximately $1.5 \times (R^{\mathrm{F}}_{\mathrm{cov}} + R^{\mathrm{Si}}_{\mathrm{cov}})$, whereas in orientation 3 the H–Si bond is approximately $R^{\mathrm{H}}_{\mathrm{vdW}} + R^{\mathrm{Si}}_{\mathrm{vdW}}$. The ability of fluorine atoms form a loose covalent bond with the substrate can be rationalized by the presence of electrons in the inner shell which are not involved in the formation of any polymer bond. By contrast, hydrogen ions inside the polymer can only form weak van der Waals interactions with the substrate.

Based on this model, we evaluate the rotationally averaged equilibrium surface–monomer separation a for different substrate materials on the basis of the known atomic radii.

The van-der-Waals and covalent radii used for evaluating the equilibrium distances between various substrates and monomeric ECTFE are given in Tab. 1. For each substrate, we consider 3 possible orientation of the monomer unit with respect to the substrate surface. For the orientations 1 (parallel to the surface) and 2 (with the F-end of the monomer facing the surface), the fluorine atom is the closest to the surface and we use $1.5 \times (R^{\mathrm{F}}_{\mathrm{cov}} + R^{\mathrm{X}}_{\mathrm{cov}})$ as an estimation of the separation. For orientation 3 (with the H-end of monomer facing the surface), the sum of van-der-Waals radii H–X, $R^{\mathrm{H}}_{\mathrm{VdW}} + R^{\mathrm{X}}_{\mathrm{VdW}}$, is evaluated as the separation. For glass, the distance has been calculated for Si and O atoms separately and then weighted with the stoichiometric ratio 1:2. Note that the ratio of atoms in the surface layer might deviate from this value. As the atomic parameters for Fe and Cr atoms are very similar, the particular content of Cr dopant in steel was irrelevant to the determination of the equilibrium distance. The evaluation details are summarized in Tab. 2.

Table 1: **Van der Waals and covalent radii.** Van der Waals and covalent radii of atoms used for estimating the equilibrium distance between substrate and monomeric ECTFE. For Fe and Cr, the van-der-Waals radius of Ni is taken.

Atom	R_{VdW}[A]	R_{cov}[A]
H	1.20	0.38
F	1.47	0.71
Si	2.10	1.11
O	1.52	0.73
Au	1.66	1.44
Fe	1.65	1.25
Cr	1.65	1.27

Table 2: **Equilibrium separations.** Evaluation of equilibrium separations between rotationally averaged ECTFE monomers and different substrates.

Silicon					
Orientation	Bond	Type	Sum of radii	QC results	Scaling coefficients
1	F-Si	cov.	1.82	2.84	1.6
2	F-Si	cov.	1.82	2.84	1.5
3	H-Si	VdW	3.30	3.55	1.1
Orientational average					2.93
Gold					
Orientation	Bond	Type	Sum of radii	Scaled sum	
1	F-Au	cov.	2.15	3.23	
2	F-Au	cov.	2.15	3.23	
3	H-Au	VdW	2.86	2.86	
Orientational average					3.16
Glass					
1	F-O	cov.	1.44	2.16	
2	F-O	cov.	1.44	2.16	
3	H-O	VdW	2.72	2.72	
Orientational average for O					2.25
Stoichiometric average					2.48
Steel					
1	F-Fe	cov.	1.96	2.94	
2	F-Fe	cov.	1.96	2.92	
3	H-Fe	VdW	2.85	2.85	
Orientational average					2.93

C: Material Constants

We start from optical data and eventually want to fit the various materials' permittivity with a model for their electromagnetic response. The permittivity ε and the dimensionless polarisability $\bar{\alpha}$ of a material are related via the Clausius–Mossotti law [27],

$$\bar{\alpha} = \frac{\eta}{\varepsilon_0}\,\alpha = 3\,\frac{\varepsilon - 1}{\varepsilon + 2} \quad . \tag{1}$$

Here, η is the number density of particles in the bulk material. For ECTFE, one has $\eta = 7 \cdot 10^{27}\mathrm{m}^{-3}$. Spectroscopic measurements provide the real and imaginary parts of a material's refractive index n, tabulated for real frequencies. They are related to the real and imaginary parts of the material's permittivity via $\varepsilon = n^2$. According to the Kramers-Kronig relations [27], the latter can then be used to find the (purely real) permittivity on the imaginary-frequency axis by calculating an integral

$$\varepsilon(i\omega) = 1 + \frac{2}{\pi}\int_0^\infty d\omega'\,\frac{\omega'\,\mathrm{Im}\,\varepsilon(\omega')}{\omega'^2 + \omega^2}\,. \tag{2}$$

If one transition dominates the dispersive properties of the material, the permittivity may be described by a single-resonance Drude-Lorentz model:

$$\varepsilon(\omega) = 1 + \frac{\omega_\mathrm{P}^2}{\omega_\mathrm{T}^2 - \omega^2 - \mathrm{i}\gamma\omega}\,. \tag{3}$$

Here, the plasma frequency ω_P describes the strength of the resonance, the transverse frequency ω_T its position on the real-frequency axis and γ its width. The free electrons contained in metals have zero transverse frequency. For materials with a more complex dielectric response, multi-resonance models may be employed. For dielectrics all resonances are located at finite frequencies. If they are well separated from each other, the corresponding single-resonance response functions may simply be added. For metals, one of the resonances is

located at zero frequency, so the following product model is advantageous:

$$\varepsilon(\omega) = \frac{\omega_{\mathrm{L}_1}^2 - \omega^2 - i\gamma_{\mathrm{L}_1}\omega}{-\omega^2 - i\gamma_{\mathrm{T}_1}\omega} \cdot \frac{\omega_{\mathrm{L}_2}^2 - \omega^2 - i\gamma_{\mathrm{L}_2}\omega}{\omega_{\mathrm{T}_2}^2 - \omega^2 - \mathrm{i}\gamma_{\mathrm{T}_2}\omega} \,. \tag{4}$$

The two different widths γ_{L} and γ_{T} facilitate a modelling of dispersion profiles with asymmetric peaks.

Finally, we note that some of the studied materials are composite. In this case, the dimensionless polarisability of the compound is the sum of the polarisabilities of the individual ingredients, weighted by the respective particle number fractions. Defining said fraction for a given material as

$$q_j = \frac{\eta_j}{\sum_k \eta_k} \qquad \text{with } \sum_j q_j = 1 \,, \tag{5}$$

the effective polarisability of the compound is given by

$$\bar{\alpha} = \sum_j q_j \bar{\alpha}_j \,. \tag{6}$$

Stainless steel is a composite material consisting mainly of iron (Fe,84.7%) and chromium (Cr, 15.3%). The parameters obtained by fitting the aforementioned models to the optical data of the materials under study can be found in Tab. 3.

Table 3: **Fit parameters.** Fit parameters for the materials studied. The upper three rows, i.e. metal parameters, refer to composite model (4), while the lower three rows, i.e. metalloids and dielectrics, were fitted with the Drude-Lorentz model (3).

	$\omega_{\mathrm{T}}\,[10^{15}\frac{\mathrm{rad}}{\mathrm{s}}]$	$\omega_{\mathrm{L}}\,[10^{15}\frac{\mathrm{rad}}{\mathrm{s}}]$	$\gamma_{\mathrm{T}}\,[10^{14}\frac{\mathrm{rad}}{\mathrm{s}}]$	$\gamma_{\mathrm{L}}\,[10^{14}\frac{\mathrm{rad}}{\mathrm{s}}]$
Gold	– 4.3	3.8 13	0.83 38	7.9 350
Iron	– 4.5	26 8.2	27 1800	1100 740
Chromium	– 3.0	1.0 18	.55 37	15 270
	$\omega_{\mathrm{T}}\,[10^{15}\frac{\mathrm{rad}}{\mathrm{s}}]$	$\omega_{\mathrm{P}}\,[10^{15}\frac{\mathrm{rad}}{\mathrm{s}}]$	$\gamma\,[10^{14}\frac{\mathrm{rad}}{\mathrm{s}}]$	$\varepsilon(0)$
ECTFE	27	26	72	1.93
Silicon dioxide	0.13 27	1.7 29	0.43 81	3.91
Silicon	71	23	9.8	11.7

D: Hamaker approximation

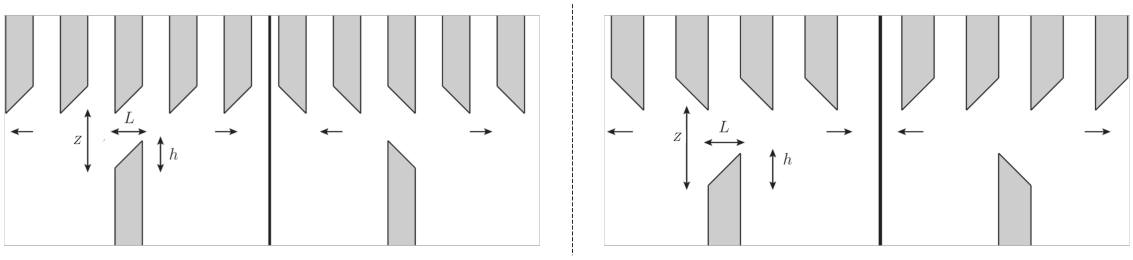

Figure 1: **Hamaker approximation.** Left: Contributions to U_1/A in the Hamaker approach. Right: Contributions to U_2/A in the Hamaker approach.

The Hamaker approximation [30] reproduces the two-body contribution to the geometry-dependence. We hence calculate:

$$U = -\eta_{\mathrm{ECTFE}}\eta_{\mathrm{sub}} \int_{V_1} \mathrm{d}^3 r_1 \int_{V_2} \mathrm{d}^3 r_2 \frac{C_6}{|\mathbf{r}_1 - \mathbf{r}_2|^6} \tag{7}$$

where $C_6 = -\frac{3\hbar}{16\pi^3\varepsilon_0^2}\int_0^\infty d\omega \alpha_{\mathrm{ECTFE}}(i\omega)\,\alpha_{\mathrm{sub}}(i\omega)$ and η_{ECTFE}, η_{sub} represent the number-densities of the ECTFE film and the substrate. Using this approximation the parameter λ, which is the ratio between the force and the force for flat surfaces, can be evaluated. To

evaluate the double integral (7), we decompose the two corrugated structures into sections as indicated in Figs. 1. One reads off for the energy per unit area:

$$\frac{U}{A} = \sum_{n=-\infty}^{\infty} \left(\frac{U_1^n}{A} + \frac{U_2^n}{A} \right), \tag{8}$$

where

$$\frac{U_1^n}{A} = -\eta_{\mathrm{ECTFE}}\eta_{\mathrm{sub}} \frac{1}{L} \int_0^L dx_1 \int_{-\infty}^{f_1(x_1)} dz_1 \int_{2mL}^{2mL+L} dx_2 \int_{-\infty}^{\infty} dy_2 \int_{z+f_2(x_2)}^{\infty} dz_2 \frac{C_6}{|\vec{r}_1 - \vec{r}_2|^6}\,, \tag{9}$$

$$\frac{U_2^n}{A} = -\eta_{\mathrm{ECTFE}}\eta_{\mathrm{sub}} \frac{1}{L} \int_0^L dx_1 \int_{-\infty}^{f_1(x_1)} dz_1 \int_{2mL+L}^{2mL+2L} dx_2 \int_{-\infty}^{\infty} dy_2 \int_{z+f_3(x_2)}^{\infty} dz_2 \frac{C_6}{|\vec{r}_1 - \vec{r}_2|^6}\,. \tag{10}$$

The functions $f_1(x_1) = \frac{h}{L}x_1$, $f_2(x_2) = \frac{h}{L}x_2 - 2mh$ and $f_3(x_2) = 2(m+1)h - \frac{h}{L}x_2$ describe the roughness profiles of the surfaces. For flat surfaces we obtain the well-known result $\frac{U}{A} = -\frac{C_3^{\mathrm{pw}}}{2z^2}$, where $C_3^{\mathrm{pw}} = \frac{\pi}{6}\eta_{\mathrm{ECTFE}}\eta_{\mathrm{sub}}C_6$. The dominant term in the energy for small a is represented by the term $\frac{U_1^0}{A}$, we have numerically verified that the other terms represent small corrections. The integration gives:

$$\begin{aligned}\frac{U_1^0}{A} = -\frac{C_3^{\mathrm{pw}}}{8L^4z^2}\Bigg\{ & L\left(2h^3 + 3hL^2 - 6h^2z - 3L^2z\right) \\ & - 2L\left[-3hz^2 + z^3 - \left(h^2 + L^2 - 2hz + z^2\right)^{3/2}\right] + \\ & + L\left[(2h^2 + 2L^2 + 4hz + 2z^2)\sqrt{L^2 + (h+z)^2} - (h+z)(3L^2 + 2(h+z)^2)\right]\Bigg\}\end{aligned} \tag{11}$$

The corresponding force can be expressed in terms of the parameters θ, a and L via $h =$

$l/\tan\theta$, $z = a/\sin\theta$:

$$\frac{f_0^1(\theta,a,L)}{A} = -\frac{C_3^{\mathrm{pw}}}{6a^3L^3\sqrt{L^2+(L\cot\theta+a\csc\theta)^2}}$$
$$\times\Bigg[-2aL(a^2-5L^2)\cot\theta+2\left(-a^4+2a^2L^2+2L^4+a^2L^2\cos 2\theta\right)\csc\theta$$
$$+\csc\theta\sqrt{(a^2+L^2+2aL\cos\theta)}\Big(4a^3-9aL^2-3aL^2\cos 2\theta-2(a^2-2L^2+aL\cos\theta)$$
$$+\sqrt{(a^2+L^2-2aL\cos\theta)\csc^2\theta}\sin\theta\Big)\Bigg]. \quad (12)$$

The roughness correction factor is then given by

$$\lambda(\theta,a,L) = \frac{f_0^1(\theta,a,L)}{f_0^1(\pi/2,a,L)}. \quad (13)$$